Atmos. Chem. Phys. Discuss., doi:10.5194/acp-2017-425, 2017
Manuscript under review for journal Atmos. Chem. Phys.
Discussion started: 19 May 2017

Atmospheric Chemistry and Physics Discussions

Equatorward dispersion of high-latitude volcanic plume and its relation to the Asian summer monsoon: a case study of the Sarychev eruption in 2009

Xue Wu[1,2], Sabine Griessbach[1], Lars Hoffmann[1]

[1]Jülich Supercomputing Centre, Forschungszentrum Jülich, Jülich, Germany
[2]Key Laboratory of Middle Atmosphere and Global Environment Observation, Institute of Atmospheric Physics, Chinese Academy of Sciences, Beijing, China

Correspondence to: Xue Wu (xu.wu@fz-juelich.de)

Abstract.

Tropical volcanic eruptions have been widely studied for their significant contribution to the stratospheric aerosol loading and global climate impacts, but the impact of high-latitude volcanic eruptions on the stratospheric aerosol layer is not clear and the pathway of transporting aerosol from high-latitudes to the tropical stratosphere is not well understood. In this work, we focus on the high-latitude volcano Sarychev (48.1°N, 153.2°E), which erupted during the Asian summer monsoon (ASM) season in 2009, and the influence of ASM on the equatorward dispersion of the volcanic plume. First, the sulfur dioxide (SO_2) emission rate and plume height of the Sarychev eruption are estimated with SO_2 observations of the Atmospheric Infrared Sounder (AIRS) and a backward trajectory approach, using the Lagrangian particle dispersion model Massive–Parallel Trajectory Calculations (MPTRAC). Then, the transport and dispersion of the plume are simulated using the derived emission rate time series. The transport simulations are compared with SO_2 observations from AIRS and validated with aerosol observations from the Michelson Interferometer for Passive Atmospheric Sounding (MIPAS). The simulations show that about 4% of the emissions were transported to the tropical stratosphere within 50 days after the beginning of the eruption, and the plume dispersed towards the tropical tropopause layer (TTL) through isentropic transport above the subtropical jet. The simulations and MIPAS aerosol data both show that in the vertical range of 360–400 K, the equatorward transport was primarily driven by anticyclonic Rossby wave breaking enhanced by the ASM in boreal summer. The volcanic plume was entrained along the anticyclone flows and reached the TTL as it was transported south-westwards into the deep tropics downstream of the anticyclone. Further, the ASM anticyclone influenced the pathway of aerosols by isolating an 'aerosol hole' inside of the ASM, which was surrounded by aerosol-rich air outside. This transport barrier was best indicated using the potential vorticity gradient approach. Long-term MIPAS aerosol detections show that after entering the TTL, the aerosol from the Sarychev eruption remained in the tropical stratosphere for about 10 months and ascended slowly. The ascent speed agreed well with the ascent speed of water vapour tape recorder. In contrast, by running a hypothetical simulation for a wintertime eruption, it is confirmed that under winter circulations, the equatorward transport of the plume would be suppressed by the strong subtropical jet and weak wave breaking events. In this hypothetic scenario, high-latitude volcanic eruption would not be able to contribute to the tropical stratospheric aerosol layer.

Atmos. Chem. Phys. Discuss., doi:10.5194/acp-2017-425, 2017
Manuscript under review for journal Atmos. Chem. Phys.
Discussion started: 19 May 2017

Atmospheric Chemistry and Physics Discussions

1 Introduction

The impact of volcanic aerosol on climate has received wide attention over decades. Robock (2000, 2013) give a comprehensive review on this subject. The major sources of the stratospheric aerosol are volcanic sulfur gases, mainly in form of SO_2, which are oxidized and converted into sulfate aerosol within hours to weeks (von Glasow et al., 2009). The sulfate aerosol is responsible for profound effects on the global climate (McCormick et al., 1995; Robock, 2000). Sulfate aerosol is a strong reflector of visible solar radiation and causes cooling of the troposphere for years; while it is also an effective absorber of near infrared solar radiation and may induce heating of the stratosphere. In contrast, H_2O and CO_2 in the volcanic emissions do not have much measureable impact on the global climate since they are less abundant than atmospheric H_2O and CO_2 reservoir (Gerlach, 1991; Gerlach, 2011). Volcanic ash usually only causes regional influence on climate for weeks, because of its large particle size, fast sedimentation, and consequently short life time in atmosphere (Niemeier et al., 2009).

The stratospheric aerosol layer enhanced by volcanism not only has a significant impact on the Earth's radiative budget (McCormick et al., 1995; Robock, 2000), it also has an impact on chemical processes in the lower stratosphere (Rodriguez et al., 1991; Solomon et al., 1993), in particular, on ozone depletion (Jäger and Wege, 1990; Tilmes et al., 2008; Solomon et al., 2016). Conventionally, large volcanic eruptions with a volcanic explosivity index (VEI) larger than 4, are thought to play a key role in the stratospheric sulfate aerosol budget. Recently, several studies focused on small and moderate-sized volcanic eruptions (VEI $\leq$ 4) (Kravitz et al., 2011; Solomon et al., 2011; Vernier et al., 2011; Ridley et al., 2014) and considered them as the primary source of the notable increase of stratospheric aerosol since 2000 that slowed down global warming (Solomon et al., 2011; Neely et al., 2013; Haywood et al., 2014). Models neglecting the effects of less intense volcanic eruptions tend to overestimate the tropospheric warming (Santer et al., 2014). The potential climate impact of volcanic emissions also largely depends on the time of year when the eruption takes place, the injection height and the surrounding meteorological conditions (Kravitz et al., 2011). The season influences sulfate formation and the zonal asymmetry of the polar vortex can affect the aerosol's transport. The eruption plume height is fundamental for aerosol microphysics in the atmosphere and the large scale circulations affect the transport of the plume. So instead of only using the VEI, it is more sensible to study the atmospheric impacts by including volcanic eruptions based on the amount of stratospheric SO_2 injection together with eruption height (Brühl et al., 2015; Timmreck, 2012). Further information on volcanic SO_2 emissions and plume altitudes are crucial in climate models when estimating trends of global temperature or ozone depletion.

The majority of studies on global climate impact of volcanic eruptions focuses on tropical eruptions. Extratropical volcanic eruptions are expected to have less impact on the global climate, because the downward flow of the Brewer–Dobson circulation in the stratospheric extra-tropics prevents sulfate aerosol from rising up (Seviour et al., 2012), and sulfate aerosol in the extratropical stratosphere easily subsides back to the troposphere within months (Holton et al., 1995; Kremser et al., 2016). Although some studies show that extratropical volcanic eruptions can also have a significant impact on climate (Highwood and Stevenson, 2003; Oman et al., 2005; Oman et al., 2006; Kravitz and Robock, 2011; Pausata et al., 2015a; Pausata et al., 2015b), the impact is usually found to be limited to the specific hemisphere in which the eruption occurred (Graf and Timmreck, 2001; Kravitz and Robock, 2011; Pausata et al., 2015b).

However, a high-latitude volcanic eruption may also contribute to the tropical stratospheric aerosol loading and even affect the other hemisphere (Schmidt et al., 2010). In this paper, we focus on the eruption of the high-

Atmos. Chem. Phys. Discuss., doi:10.5194/acp-2017-425, 2017
Manuscript under review for journal Atmos. Chem. Phys.
Discussion started: 19 May 2017

Atmospheric Chemistry and Physics Discussions

latitude volcano, Sarychev in 2009, which is considered as one of the high-latitude eruptions that affect tropical latitudes (von Savigny et al., 2015) and are responsible for the increase in tropical stratospheric aerosol optical depth. In particular, we study the transport pathway of the Sarychev aerosol from the extra-tropical lower stratosphere to the TTL. In order to analyse the transport of the Sarychev plume and the role of the ASM in the dispersion process, in Section 2 we first present the Lagrangian transport model and data used for simulations. In Section 3, we derive the altitude-resolved Sarychev volcanic emission time series using AIRS SO_2 measurements and an inverse modelling approach. The equatorward dispersion of the Sarychev emissions revealed by MIPAS aerosol detections and trajectory simulations and the relation to ASM are shown in Section 4. Results of this study are further discussed in Section 5 and summarized in Section 6.

2 Observations and model

2.1 AIRS

AIRS (Aumann et al., 2003) is an infrared sounder with across-track scanning capabilities aboard the National Aeronautics and Space Administration's (NASA's) Aqua satellite. Aqua was launched in May 2002 and operates in a nearly polar, Sun-synchronous orbit at an altitude of about 710 km with a period of 98 min. The AIRS footprint size is 13.5 km×13.5 km for nadir and 41 km×21.4 km for the outermost scan angles. The along-track distance between two adjacent scans is 18 km. AIRS provides nearly continuous measurement coverage during 14.5 orbits per day and covers the globe almost twice a day. The observations provide good horizontal resolution and make it ideal data for observing the fine filamentary structures of volcanic SO_2 plumes.

In this study, we use an SO_2 index defined by brightness temperature differences (BTDs) based on SO_2 spectral features in the 7.3 µm waveband (Hoffmann et al., 2014) to estimate emission rates and evaluate the Lagrangian transport simulations. The SO_2 index increases with increasing SO_2 column density and it is most sensitive to SO_2 at altitudes from 8 to 13 km. The SO_2 index of Hoffmann et al. (2014) performs better on suppressing background signals than the SO_2 index provided in the NASA operational data products. It is therefore well suited to track low SO_2 concentrations over time. In this work, we applied a detection threshold of 2 K for the SO_2 index to identify volcanic emissions.

AIRS was able to detect the SO_2 cloud from the beginning of the eruption of Sarychev on 12 June 2009 up to five weeks later. Observations during the first five days after the eruption have been used for estimating the emission rates. Observations at a later stage are used for comparison with the Lagrangian transport simulations.

2.2 MIPAS

MIPAS (Fischer et al., 2008) is an infrared limb emission spectrometer aboard European Space Agency's (ESA's) Envisat, which was in operation from July 2002 to April 2012, providing nearly 10 years of measurements. The vertical coverage of its nominal mode was 7–72 km from January 2005 to April 2012. MIPAS has a field of view of about 3 km×30 km (vertically and horizontally) at the tangent point and dimension of the measurement volume along the line of sight is about 300 km. The horizontal distance between two adjacent limb scans is about 500 km. In 2009, the general measurement pattern of MIPAS is to measure eight days in nominal mode followed by one day in middle atmosphere mode and one day in upper atmosphere

mode. On each day, about 14 orbits with about 90 profiles per orbit are measured. From January 2005 to April 2012, the vertical sampling grid spacing between the tangent altitudes is 1.5 km in the UTLS and 3 km above.

In this study, we use MIPAS altitude-resolved aerosol data (Griessbach et al., 2016). In the first step, we used the aerosol-cloud-index to identify cloud or aerosol contaminated spectra, and in the second step we use a brightness temperature correction method to separate aerosol from ice clouds. The resulting aerosol product may contain any type of aerosol, e.g. volcanic ash, sulfate aerosol, mineral dust as well as non-ice polar stratospheric clouds (PSCs). MIPAS detected Sarychev aerosol starting on 13 June 2009.

2.3 MPTRAC

The Massive-Parallel Trajectory Calculations (MPTRAC) model is Lagrangian particle dispersion model, which is particularly suited to study volcanic eruption events (Heng et al., 2015; Hoffmann et al., 2016). In the MPTRAC model, trajectories for individual air parcels are calculated based on numerical integration of the kinematic equation of motion and simulations are driven by wind fields from global meteorological reanalyses. Turbulent diffusion is modelled by uncorrelated Gaussian random displacements of the air parcels with zero mean and standard deviations $\sigma_x = \sqrt{D_x \Delta t}$ (horizontally) and $\sigma_z = \sqrt{D_z \Delta t}$ (vertically). D_x and D_z are the horizontal and vertical diffusivities respectively, and Δt is the time step for the trajectory calculations. For the Sarychev simulation, D_x is assigned to be 50 $m^2 s^{-1}$ in the troposphere and D_z is assigned to be 0.1 $m^2 s^{-1}$ in the stratosphere following Stohl et al. (2005). Furthermore, the sub-grid scale wind fluctuations are simulated by a Markov model (Stohl et al., 2005; Hofmann et al., 2016). Loss processes of chemical species, SO_2 in our simulations, are simulated based on an exponential decay of the mass assigned to each air parcel, with a constant half lifetime of seven days.

In this study, the MPTRAC model is driven with the ERA–Interim data (Dee et al., 2011) interpolated on a 1°× 1° horizontal grid on 60 model levels with the vertical range extending from the surface to 0.1 hPa. The ERA–Interim data is provided at 0000, 0600, 1200, and 1800 UTC.

3 Simulations and observations of the Sarychev plume

3.1 Reconstruction of the Sarychev SO_2 emission time series

The Sarychev peak with summit at 1496 m, is located at 48.1°N, 153.2°E, and it is one of the most active volcanoes of the Kuril Islands. It erupted most recently in June 2009 (VEI = 4). On 11 June 2009, two weak ash eruptions were first detected (Levin et al., 2010) and during the main explosive phase from 12 to 16 June 2009, ash, water vapour, and an estimated 1.2±0.2 Tg of SO_2 were injected into the UTLS, making it one of the 10 largest stratospheric injections in the last 50 years (Haywood et al., 2010). Sulfate aerosol was detected several days after the eruption and the enhancement of the optical depth caused by the Sarychev eruption lasted for months, returning to pre-Sarychev eruption values in the beginning of 2010 (Doeringer et al., 2012; Jégou et al., 2013). As shown in Fig. 1 (top), Sarychev is located at the northern edge of the subtropical jet and to the northeast of the ASM (marked by the black rectangle). In the vertical section (Fig. 1, bottom), the dynamical tropopause, defined by a potential vorticity (PV) value of 2 PV units (PVU), is around 11 km at the location of the Sarychev.

Atmos. Chem. Phys. Discuss., doi:10.5194/acp-2017-425, 2017
Manuscript under review for journal Atmos. Chem. Phys.
Discussion started: 19 May 2017

Atmospheric Chemistry and Physics Discussions

To reconstruct the altitude-resolved SO_2 emission time series, we follow the approach of Hoffmann et al. (2016) and use backward trajectories and AIRS SO_2 measurements. Since AIRS measurements do not provide altitude information, we establish a column of air parcels at each location of an AIRS SO_2 detection. The vertical range of the column is 0–25 km, covering the possible vertical dispersion range of the SO_2 plume in the first few days. The AIRS footprint size varies between 14 and 41 km, so in the horizontal direction we choose an average of 30 km as the full width at half maximum (FWHM) for the Gaussian scatter of the air parcels. In our simulation, a fixed number of 100,000 air parcels is assigned to all air columns and the number of air parcels in each column is linearly proportional to the SO_2 index. Then backward trajectories were calculated for all air parcels, and trajectories that are at least 2 days but no more than 5 days long and that have passed the volcano domain are recorded as emissions of Sarychev. The volcano domain is defined to be within a radius of 75 km to the location of Sarychev and 0–20 km in the vertical direction, covering all possible injection heights. Sensitivity experiments have been conducted to optimize these pre-assigned parameters to obtain best simulation results. Haywood et al. (2010) estimated that 1.2 Tg of SO_2 were injected into the UTLS on 15 and 16 June 2009 with a 15 % error estimate (± 0.2 Tg). Considering that there were minor emissions before 15 June (Levin et al., 2010; Jégou et al., 2013; Carboni et al., 2016), we allocated a mass of 1.4 Tg to the derived SO_2 emissions. The reconstructed SO_2 emission time series is shown in Fig. 2.

In Fig. 2, black dots denote the thermal tropopause derived from ERA–interim data at the Sarychev. Sarychev released SO_2 almost without interruption in the first five days, but with large variations in height and magnitude. Smaller eruptions began on 12 June followed by continuous eruptions on 13 June, ranging from 7 km to about 17 km. Significant SO_2 injections occurred on 14–15 June between 10 and 18 km, followed by minor emissions until 16 June. The majority of SO_2 (58%, ~0.81Tg) was injected directly into the extratropical lower stratosphere, and the largest SO_2 injection occurred between 12 and 17 km. These time line of the eruptions is consistent with the observation of the Japanese Meteorological Agency Multifunctional Transport Satellite (MTSAT) (Levin et al., 2010; Rybin et al., 2011) and the Optical Spectrograph and Infrared Imaging System (OSIRIS) measurements, showing that the peak backscatter of aerosols measured were between 12 and 16 km (Kravitz et al., 2011).

The derived SO_2 emission rate time series are the basis of the simulations of SO_2 plume in the following sections.

3.2 Simulation and validation of the Sarychev plume dispersion

A new set of 100,000 air parcels is assigned to the derived SO_2 emission shown in Fig. 2, with 14,000 kg of SO_2 in each of the air parcel. The trajectories initialized with this SO_2 emission are calculated with the MPTRAC model from 12 June 2009 (first eruption) to 31 July 2009. The simulated evolution of the SO_2 plume is shown in Fig. 3 (left column) and compared with the AIRS SO_2 measurements (right column). Note that only SO_2 column density values larger than 2 Dobson units (DU) are shown. The evolution of simulated plume altitudes is shown in Fig. 4 together with tangent altitudes of the MIPAS aerosol detections. Figure 3 and Fig. 4 show that, as the SO_2 was injected into different altitudes, the SO_2 plume splited roughly into two branches after the eruption, moving eastwards and westwards, and at the same time, most of the emissions moving poleward. From 22 June, the SO_2 plume over Eastern Siberia stretched towards three directions: northeast, south, and south east. The SO_2 in the elongated filament over the Eastern Siberia and North-east China with altitudes below 9 km was

diluted and partly depleted and converted into aerosol afterwards and the other two filaments moved toward east. The SO_2 plume over the Northwest American continent stretched towards east and west, forming a long filament running through Northern Canada. The SO_2 concentration declined exponentially and only a fraction of SO_2 remained near the Bering Strait and Northern Canada till 28 June.

In Fig. 3, in order to validate the simulation of plume dispersion, and also to indirectly validate the reconstructed emission rates, we compare the simulations of plume dispersion with AIRS SO_2 measurements. The SO_2 index from AIRS detections was converted into SO_2 column density using the correlation function described in Hoffmann et al. (2014), which was built using radiative transfer calculations. AIRS was able to detect the SO_2 cloud from the beginning of the eruption of Sarychev up to five weeks later (not fully shown in the figure). The SO_2 column density derived from AIRS agrees well with the SO_2 column density derived from the Infrared Atmospheric Sounding Interferometer (IASI) in magnitude, e.g. see Fig. 3 in the study of Haywood et al. (2010) and Fig. 2 in the study of Jégou et al. (2013). Generally, the simulations agree well with the AIRS measurements in position and diffusion and the simulations can provide more information on the SO_2 distribution than the AIRS measurements alone. The differences between the SO_2 clouds, e.g. on 24 June (over the western Pacific) are partly attributed to a mismatch in time of the AIRS SO_2 measurements and the simulation output. In magnitude, the SO_2 column density from AIRS is slightly larger than that from MPTRAC simulations, and the SO_2 maxima are found in different location. This is also found by Hoffmann et al. (2016) for other eruption events and this was attributed to the fact that the inverse modelling approach is optimized to reproduce the spatial extent of the plume but not the absolute emission. Except for discrepancy between the times of the compared data, this remaining difference may also be attributed to the initial setting of the total SO_2 mass, the SO_2 life time and the uncertainties of the ECMWF-interim winds.

In Fig. 4, the altitudes of the simulated SO_2 plume are compared with the tangent altitudes of MIPAS aerosol detections to verify the vertical distribution of the SO_2 plume. Aerosol produced by the Sarychev eruption was detected by MIPAS within a few days after the initial eruption. In general, the altitudes of the simulated SO_2 plume are comparable to the MIPAS aerosol altitudes. The majority of the air parcels were between 10 and 20 km and moved eastwards. A thin filament over the north Pacific ascended to up to 20 km and moved westward to East Asia by the end of June 2009, which was well verified by the MIPAS detections. Some apparent inconsistencies, e.g., along the west coast of North American on 23 June and over the northeast Pacific on 24 and 25 June. We attributed it to the fact that the SO_2 at lower altitudes (below 14 km) had been converted into aerosol more quickly than the SO_2 at higher altitudes (above 16 km). The various vertical distributions of the air parcels were also verified by some overlapping MIPAS detections, e.g., over northwest America. Overall, this comparison demonstrates that the MPTRAC simulation provides a quite accurate representation of the observed horizontal and vertical distribution of the Sarychev SO_2 plume.

4 Equatorward dispersion of the Sarychev plume and the role of the ASM

4.1 Equatorward dispersion of Sarychev plume

Although the majority of the Sarychev plume was transported towards the north pole, it's found in our simulations that there was clear equatorward dispersion from extratropical stratosphere to the tropical lower stratosphere, as seen in Fig. 5 (top). The plume reached the tropical stratosphere about one week after the

eruption, and crossed the Equator by the end of June 2009. Till the end of July 2009, there were nearly 4% of the air parcels that had entered the tropical stratosphere. This trend is further verified by the MIPAS aerosol detections (middle and bottom panels in Fig. 5). As shown by the MIPAS aerosol detections, shortly after the eruption of Sarychev, large quantities of stratospheric aerosol formed from directly injected SO_2. Most of the stratospheric aerosol stayed at Northern Hemisphere mid- and high latitudes. However, there was an increasing number of aerosol detections in the tropical stratosphere. The aerosol in the extratropical stratosphere was removed by the end of 2009, while the aerosol that had entered the tropical stratosphere stayed for months. Aerosol optical depths from OSIRIS and scattering ratio from CALIPSO lidar measurements have also shown similar equatorward dispersion of the aerosol after the eruption of Sarychev (Haywood et al., 2010; Solomon et al., 2011).

4.2 The role of the ASM anticyclone

As shown by the evolution of Sarychev plume in section 3.2, active Rossby wave breaking events at mid-latitudes during boreal summer have significantly influenced the plume dispersion. In boreal summer, the ASM is among the most prominent circulation patterns. Figure 6 shows a cross section of the ASM in boreal summer 2009. Generally, the ASM ranged from 360–400 K, marked by the negative PV anomaly of -3 and it was bounded by the subtropical and equatorial jets. The thermal tropopause averaged over 40–120°E was elevated up to about 390 K. The ASM anticyclonic circulation facilitates meridional transport when the subtropical jet weakens and retreats northward (Haynes and Shuckburgh, 2000). Figure 7 depicts the MIPAS aerosol measurements between 40–120°E during June–August 2009. The aerosol detections between 360 and 400 K were collocated with the core of the ASM, extending from the mid-latitude UTLS to the TTL. The aerosol that made their way above the subtropical jet core to lower latitudes along the isentropic surfaces cannot be explained by convection but only by large-scale transport associated with the ASM.

Using our trajectory simulations, it is straightforward to see the role of ASM anticyclonic circulation in influencing the pathway of the plume. The distributions of air parcels in the vertical range of 360–400 K (in percentage of total number of air parcels released after the eruption) by the 30 June, 10 July, 20 July and 31 July 2009 are shown in Fig. 8. The red contour is the geopotential height of 14,320 m on 150 hPa pressure surface, denoting a commonly used boundary of the ASM anticyclone (Randel and Park, 2006). At latitudes between 15–40°N in summer, the 150 hPa pressure surface is around 370 K .The black contour is the PV-based ASM transport barrier for July 2009 (1.8 PVU) on 370 K isentropic surface as defined by Ploeger et al. (2015).

In the first 19 days (top left panel in Fig. 8), from first eruption on 12 June to 30 June 2009, the plume mostly moved eastward and remained at mid- and high latitudes. After another 10 days (top right panel in Fig. 8), air parcels were entrained into the anticyclonic circulations of the American monsoon and a fraction was shed towards the tropics. The remaining air parcels that entered the ASM circulation were entrained along the flow surrounding the ASM anticyclone and moved south-westward approaching the tropics. In the following 20 days (bottom panels in Fig. 8), some air parcels were dragged along the flow south of the ASM, and some were shed out from the south-eastern flank of the anticyclone and spread over the tropics. The American monsoon plays a similar role as the ASM in transporting air parcels to lower latitudes, but it is much weaker in strength. The ‘aerosol hole’ between 360 and 400 K illustrated the ASM’s role as a transport barrier between the air inside and outside of the anticyclone. In our case, it is better demarcated by the PV-based barrier than the geopotential

height criterion. The northern barrier of the subtropical jet was strong, while the southern barrier was more permeable for meridional transport.

This meridional transport under the influence of the ASM revealed by the simulations shown in Fig. 8 is verified by the MIPAS aerosol detections shown in Fig. 9. Because of the sparse horizontal coverage of MIPAS detections, 1.5-day forward and 1.5-day backward trajectories initialized by MIPAS aerosol detections were calculated to fill gaps in space and time. Compared with MIPAS detections in Fig. 9, the simulations in Fig. 8 could successfully reproduce the maxima, minima and filaments of the aerosol distributions. It is also verified by MIPAS detections that the transport barrier of ASM is better demarcated by the PV-based barrier.

The transport pathway to low latitudes for aerosols above 400 K is shown by simulations in Fig. 10 and MIPAS aerosol detections in Fig. 11. At altitudes above the ASM, trajectories are driven by easterlies and meridional, isentropic winds. Till end of July 2009, air parcels above 400 K were transported to lower latitudes (as far as about 15°N), but could not reach the Equator. This suggests that ASM play the most significant role between 360 and 400 K, which may vary in spatial extent associated with the strength of the ASM.

However, a sensitivity test simulation of the same eruption in winter (January 2009) shows that, in northern hemisphere winter, meridional transport from extra-tropic to the tropics is typically suppressed by the strong winter subtropical jets. Forward trajectories initialized by the Sarychev SO_2 emissions (as shown in Fig. 2), but driven by winter wind fields in January and February 2009 are shown in Fig. 12. Compared with the summer scenario in Fig. 8, wind speeds in winter 2009 between 360 and 400 K were faster, and the trajectories could span the northern hemisphere within 20 days. About 40 days after eruption, air parcels were almost evenly distributed at mid- and high latitudes, but no air parcels did approach the Equator.

4.3 Upward transport of Sarychev aerosol

Simulation results from Figs. 8 to 11 have shown that the ASM anticyclone enhanced the equatorward dispersion of the Sarychev aerosol in the vertical range of 360–400 K, but the ASM did not facilitate the equatorward dispersion above 400K. The increased aerosol in the tropical stratosphere above 400 K (~ 18 km) could only be explained by the upward transport above the TTL. Above zero diabatic heating surface (generally around 360 K), air masses that enter the TTL are considered to be lifted effectively by the radiative heating (Gettelman et al., 2004; Fueglistaler et al., 2009).

In Fig. 13, the upward transport of aerosol in the tropics is clearly demonstrated by the MIPAS aerosol detections at high altitudes between 10°N and 10°S. At 15 km, an enhanced aerosol signal was found from July 2009 and lasted for about 10 months. It returned to pre-Sarychev level at the end of May 2010. At 20 km, enhanced aerosol signal was detected in October 2009, and in another four months, the enhanced aerosol signal was found at 25 km. The overlaid ascent speed of water vapour tape recorder is derived with Aura Microwave Limb Sounder (MLS) measurements from Glanville et al. (2017). The ascent speed of the Sarychev aerosol agrees well with the ascent speed of the water vapour tape recorder before and after the data gap at the end of 2009 and beginning of 2010, which can be explained since the Sarychev aerosol is mainly in form of H_2SO_4-H_2O solution. This gap in the MIPAS aerosol data is caused by semi-annual temperature variations at higher altitudes (Griessbach et al., 2016).

Atmos. Chem. Phys. Discuss., doi:10.5194/acp-2017-425, 2017
Manuscript under review for journal Atmos. Chem. Phys.
Discussion started: 19 May 2017

Atmospheric Chemistry and Physics Discussions

5 Discussion

The results of our study in above sections suggest that the ASM anticyclone plays a key role in transporting the Sarychev aerosol from extra-tropical lower stratosphere into the TTL. In various studies, this quasi-isentropic transport from extra-tropics to the TTL is referred as in-mixing process (e.g., Konopka et al., 2009). Horizontal in-mixing of tracer species has been observed (e.g. Folkins et al., 1999) or modelled (e.g. Konopka et al., 2010), and has been used to explain the seasonal and annual cycle of tracer species (Abalos et al., 2013; Ploeger et al., 2013). The role of in-mixing is prominent when there are large gradients in these tracers between the tropics and the extra-tropics. The study of Abalos et al. (2013) shows that the main contribution to in-mixing originates in the northern hemisphere and is related to the Asian monsoon, and this in-mixing process takes place in the TTL close to the tropopause. These extra-tropics to tropics transport events are also considered to be driven by anticyclonic Rossby wave breaking (Homeyer and Bowman, 2013). The net equatorward transport peaks downstream of large anticyclones in the potential temperature range between 370 and 390 K (Homeyer and Bowman, 2013). Above the TTL, in-mixing rapidly decreases with height and becomes very weak at altitudes of the tropical pipe (Ploeger et al., 2013). These findings agree well with our study, which shows that the ASM anticyclonic circulation enhanced the equatorward transport between 360 and 400 K, but not above 400 K.

The pathway of the Sarychev plume approaching the deep tropics is modulated by the transport barrier at the boundary of the ASM anticyclone as well. The 'aerosol hole' shown in Figs. 8 and 9 that ranges from 360 to 400 K and collocates with the core of ASM, only appears during the ASM season. Conventionally, the geopotential height of 14,320 m on 150 hPa is used to define the boundary of the ASM anticyclone, but from the perspective of transport, the PV-based barrier defined by Ploeger et al. (2015) can better represent the boundary.

Our results also show that the meteorological background conditions during a volcanic eruptions have a significant impact on the transport of the volcanic aerosol. For instance, the Puyehue-Cordón Caulle emissions reached the lower stratosphere and were rapidly transported eastward by the jet stream (Klüser et al, 2013; Hoffmann et al., 2016), while the Nabro emissions were captured by the ASM circulation in UTLS region (Fairlie et al., 2014; Heng et al., 2016). In this study, the transport of the equatorward dispersion of Sarychev aerosol is driven by the ASM anticyclone. Aerosol entering TTL via ASM further entered the ascending branch of the Brewer–Dobson circulation. This enabled the Sarychev aerosol to remain in the stratosphere for months and further spread over both hemispheres. In this way, the Sarychev eruption may not only influence the northern hemisphere, but could also have potential impact on the global chemical composition and radiative budget similar to a tropical volcanic eruption. Although only a fraction of the SO_2 emission (~4% out of 1.4 Tg) was transported to the tropical stratosphere by the end of July 2009, if the SO_2 is entirely converted into gaseous H_2SO_4 and condensed into a 75%-25% H_2SO_4-H_2O solution, the total aerosol mass loading added by Sarychev eruption would be about 0.07 Tg of sulfur, which is about three times larger than the 0.01–0.02 Tg of sulfur per year required to explain the average aerosol increase of 4–7 % per year after 2002 (Hofman et al., 2009). Moreover, more aerosols were transported to or ascended to the tropical stratosphere after July 2009. Although the relative change of the aerosol concentration, the SO_2 and sulfate aerosol transported to the tropics and further to the southern hemisphere will not only perturb the radiative balance but also have a substantial effect on microphysical processes, such as coagulation and growth of cloud condensation nuclei (Manktelow et al., 2009; Schmidt et al., 2010).

Since the potential climate impact of high-latitude volcanic emissions largely depends on their plume height and the meteorological background consitions, it is essential to initialize the simulations with realistic time- and altitude-resolved SO_2 emission rate. The backward trajectory approach used in this study to reconstruct the emission time series proves to be an efficient way to produce realistic SO_2 emission rate time series.

6 Summary

In this study, we analysed the equatorward transport pathway of volcanic aerosol from the high-latitude volcanic eruption of the Sarychev in 2009. The analysis was based on MIPAS aerosol detections, AIRS SO_2 measurements and trajectory simulations.

First, the time- and altitude-resolved SO_2 emission rate was derived using backward trajectories initialized with AIRS SO_2 measurements. Second, the dispersion of Sarychev plume from the beginning of the eruption (12 June 2009) to 31 July 2009 was simulated based on the derived SO_2 emissions rate. The horizontal distribution of the plume and its altitudes were validated with AIRS SO_2 measurements and MIPAS aerosol measurements respectively. The comparisons showed that there was good agreement between the simulations and observations.

The results presented in this study suggest that in boreal summer, the transport and dispersion of volcanic emissions were greatly influenced by the dominating ASM circulation, which facilitates the meridional transport of aerosols from the extra-tropical UTLS to the TTL by entraining air along the anticyclonic flows and shedding the air to the deep tropics downstream of the anticyclonic circulation. Meanwhile, the ASM anticyclone effectively isolates the air inside of the ASM from aerosol-rich air outside the anticyclone. The transport barrier at the boundary of the ASM is better denoted by the barrier defined by the PV gradient approach. However, the ASM only influenced the plume dispersion significantly in the vertical range of 360–400 K. The ASM anticyclone did not have notable impact on the equatorward dispersion above 400 K, where the Sarychev aerosol was confined in the northern hemisphere.

The simulations show that until the end of July 2009, about 4% of the emission had entered the tropical stratosphere. Increased number of aerosol was detected by MIPAS in the tropical stratosphere afterwards. After entering the TTL, the aerosol experienced large-scale ascent in the Brewer–Dobson circulation. The ascent speed agrees well with the ascent speed of the water vapour tape recorder. Aerosol signal in the tropics was enhanced within one month of the eruption, and returned to pre-Sarychev level after about 10 months.

The Sarychev eruption had the chance to contribute to the stratospheric aerosol loading in the tropics because it occurred in boreal summer when the equatorward transport was enhanced by the ASM anticyclone. If the eruption happened in winter, the volcanic aerosol would be confined to the latitudes of strong subtropical jets.

7 Code and data availability

AIRS data are distributed by the NASA Goddard Earth Sciences Data Information and Services Center (AIRS Science Team and Chahine, 2007). Envisat MIPAS Level-1B data are distributed by the European Space Agency. The ERA–Interim reanalysis data were obtained from the European Centre for Medium-Range Weather Forecasts. The code of the Massive-Parallel Trajectory Calculations (MPTRAC) model is available under the terms and conditions of the GNU General Public License, Version 3 from the repository at https://github.com/slcs-jsc/mptrac (last access: 12 April 2017).

8 Competing interests

The authors declare that they have no conflict of interest.

Acknowledgements. This work was supported by National Natural Science Foundation of China under grant No. 41605023 and International Postdoctoral Exchange Fellowship Program 2015 under grant No. 20151006. The PV gradient based transport barrier data is provided by Dr. Felix Ploeger from Institute of Energy and Climate Research: Stratosphere (IEK-7), Forschungszentrum Jülich GmbH.

References

Abalos, M., Ploeger, F., Konopka, P., Randel, W., and Serrano, E.: Ozone seasonality above the tropical tropopause: reconciling the Eulerian and Lagrangian perspectives of transport processes, Atmos. Chem. Phys., 13, 10787-10794, doi:10.5194/acp-13-10787-2013, 2013.

Aumann, H. H., Chahine, M. T., Gautier, C., Goldberg, M. D., Kalnay, E., McMillin, L. M., Revercomb, H., Rosenkranz, P. W., Smith, W. L., Staelin, D. H., Strow, L. L., and Susskind, J.: AIRS/AMSU/HSB on the Aqua mission: design, science objectives, data products, and processing systems, IEEE Trans. Geosci. Remote Sens., 41, 253-264, doi: 10.1109/TGRS.2002.808356, 2003.

Brühl, C., Lelieveld, J., Tost, H., Höpfner, M., and Glatthor, N.: Stratospheric sulfur and its implications for radiative forcing simulated by the chemistry climate model EMAC, Journal of Geophysical Research: Atmospheres, 120, 2103-2118, doi: 10.1002/2014JD022430, 2015.

Butchart, N., Scaife, A. A., Bourqui, M., de Grandpre, J., Hare, S. H. E., Kettleborough, J., Langematz, U., Manzini, E., Sassi, F., Shibata, K., Shindell, D., and Sigmond, M.: Simulations of anthropogenic change in the strength of the Brewer-Dobson circulation, Climate Dynam., 27, 727-741, 10.1007/s00382-006-0162-4, 2006.

Carboni, E., Grainger, R. G., Mather, T. A., Pyle, D. M., Thomas, G. E., Siddans, R., Smith, A. J. A., Dudhia, A., Koukouli, M. E., and Balis, D.: The vertical distribution of volcanic SO2 plume measured by IASI, Atmos. Chem. Phys., 16, 4343-4367, doi: 10.5194/acp-16-4343-2016, 2016.

Dee, D. P., Uppala, S. M., Simmons, A. J., Berrisford, P., Poli, P., Kobayashi, S., Andrae, U., Balmaseda, M. A., Balsamo, G., Bauer, P., Bechtold, P., Beljaars, A. C. M., van de Berg, L., Bidlot, J., Bormann, N., Delsol, C., Dragani, R., Fuentes, M., Geer, A. J., Haimberger, L., Healy, S. B., Hersbach, H., Hólm, E. V., Isaksen, L., Kållberg, P., Köhler, M., Matricardi, M., McNally, A. P., Monge-Sanz, B. M., Morcrette, J. J., Park, B. K., Peubey, C., de Rosnay, P., Tavolato, C., Thépaut, J. N., and Vitart, F.: The ERA-Interim reanalysis: configuration and performance of the data assimilation system, Q. J. R. Meteorol. Soc., 137, 553-597, doi: 10.1002/qj.828, 2011.

Doeringer, D., Eldering, A., Boone, C. D., González Abad, G., and Bernath, P. F.: Observation of sulfate aerosols and SO2 from the Sarychev volcanic eruption using data from the Atmospheric Chemistry Experiment (ACE), J. Geophys. Res. Atmos., 117, D03203, doi: 10.1029/2011JD016556, 2012.

Fadnavis, S., Semeniuk, K., Pozzoli, L., Schultz, M. G., Ghude, S. D., Das, S., and Kakatkar, R.: Transport of aerosols into the UTLS and their impact on the Asian monsoon region as seen in a global model simulation, Atmos. Chem. Phys., 13, 8771-8786, doi: 10.5194/acp-13-8771-2013, 2013.

Fairlie, T. D., Vernier, J. P., Natarajan, M., and Bedka, K. M.: Dispersion of the Nabro volcanic plume and its relation to the Asian summer monsoon, Atmos. Chem. Phys., 14, 7045-7057, doi: 10.5194/acp-14-7045-2014, 2014.

Fischer, H., Birk, M., Blom, C., Carli, B., Carlotti, M., von Clarmann, T., Delbouille, L., Dudhia, A., Ehhalt, D., Endemann, M., Flaud, J. M., Gessner, R., Kleinert, A., Koopman, R., Langen, J., López-Puertas, M., Mosner, P., Nett, H., Oelhaf, H., Perron, G., Remedios, J., Ridolfi, M., Stiller, G., and Zander, R.: MIPAS: an instrument for atmospheric and climate research, Atmos. Chem. Phys., 8, 2151-2188, doi: 10.5194/acp-8-2151-2008, 2008.

Folkins, I., Loewenstein, M., Podolske, J., Oltmans, S. J., and Proffitt, M.: A barrier to vertical mixing at 14 km in the tropics: Evidence from ozonesondes and aircraft measurements, J. Geophys. Res. Atmos., 104, 22095-22102, doi: 10.1029/1999JD900404, 1999.

Fueglistaler, S., Dessler, A. E., Dunkerton, T. J., Folkins, I., Fu, Q., and Mote, P. W.: Tropical Tropopause Layer, Rev. Geophys., 47, 31, doi: 10.1029/2008rg000267, 2009.

Gerlach, T.: Volcanic versus anthropogenic carbon dioxide, Eos, Trans. Am. Geophys. Union, 92, 201-202, doi: 10.1029/2011EO240001, 2011.

Gerlach, T. M.: Present-day CO2 emissions from volcanos, Eos, Trans. Am. Geophys. Union, 72, 249-255, doi: 10.1029/90EO10192, 1991.

Gettelman, A., Forster, P. M. d. F., Fujiwara, M., Fu, Q., Vömel, H., Gohar, L. K., Johanson, C., and Ammerman, M.: Radiation balance of the tropical tropopause layer, J. Geophys. Res. Atmos., 109, D07103, doi: 10.1029/2003JD004190, 2004.

Glanville, A. A., and Birner, T.: Role of vertical and horizontal mixing in the tape recorder signal near the tropical tropopause, Atmos. Chem. Phys., 17, 4337-4353, doi: 10.5194/acp-17-4337-2017, 2017.

Griessbach, S., Hoffmann, L., Spang, R., von Hobe, M., Müller, R., and Riese, M.: Infrared limb emission measurements of aerosol in the troposphere and stratosphere, Atmos. Meas. Tech., 9, 4399-4423, doi:10.5194/amt-9-4399-2016, 2016..

Haynes, P., and Shuckburgh, E.: Effective diffusivity as a diagnostic of atmospheric transport: 2. Troposphere and lower stratosphere, J. Geophys. Res. Atmos., 105, 22795-22810, doi: 10.1029/2000JD900092, 2000.

Haywood, J. M., Jones, A., Clarisse, L., Bourassa, A., Barnes, J., Telford, P., Bellouin, N., Boucher, O., Agnew, P., Clerbaux, C., Coheur, P., Degenstein, D., and Braesicke, P.: Observations of the eruption of the Sarychev volcano and simulations using the HadGEM2 climate model, J. Geophys. Res. Atmos., 115, D21212, doi: 10.1029/2010JD014447, 2010.

Haywood, J. M., Jones, A., and Jones, G. S.: The impact of volcanic eruptions in the period 2000–2013 on global mean temperature trends evaluated in the HadGEM2-ES climate model, Atmos. Sci. Lett., 15, 92-96, doi: 10.1002/asl2.471, 2014.

Heng, Y., Hoffmann, L., Griessbach, S., Rößler, T., and Stein, O.: Inverse transport modeling of volcanic sulfur dioxide emissions using large-scale simulations, Geosci. Model Dev., 9, 1627-1645, doi:10.5194/gmd-9-1627-2016, 2016.

Hoffmann, L., Griessbach, S., and Meyer, C. I.: Volcanic emissions from AIRS observations: detection methods, case study, and statistical analysis, in: Remote Sensing of Clouds and the Atmosphere XIX and Optics in Atmospheric Propagation and Adaptive Systems XVII, edited by: Comeron, A., Kassianov, E. I., Schafer, K., Picard, R. H., Stein, K., and Gonglewski, J. D., Proceedings of SPIE, Spie-Int Soc Optical Engineering, Bellingham, doi: 92421410.1117/12.2066326, 2014.

Hoffmann, L., Rößler, T., Griessbach, S., Heng, Y., and Stein, O.: Lagrangian transport simulations of volcanic sulfur dioxide emissions: Impact of meteorological data products, J. Geophys. Res. Atmos., 121, 4651-4673, doi: 10.1002/2015JD023749, 2016.

Hofmann, D., Barnes, J., O'Neill, M., Trudeau, M., and Neely, R.: Increase in background stratospheric aerosol observed with lidar at Mauna Loa Observatory and Boulder, Colorado, Geophys. Res. Lett., 36, L15808, doi: 10.1029/2009GL039008, 2009.

Jégou, F., Berthet, G., Brogniez, C., Renard, J. B., François, P., Haywood, J. M., Jones, A., Bourgeois, Q., Lurton, T., Auriol, F., Godin-Beekmann, S., Guimbaud, C., Krysztofiak, G., Gaubicher, B., Chartier, M., Clarisse, L., Clerbaux, C., Balois, J. Y., Verwaerde, C., and Daugeron, D.: Stratospheric aerosols from the Sarychev volcano eruption in the 2009 Arctic summer, Atmos. Chem. Phys., 13, 6533-6552, doi: 10.5194/acp-13-6533-2013, 2013.

Kremser, S., Thomason, L. W., von Hobe, M., Hermann, M., Deshler, T., Timmreck, C., Toohey, M., Stenke, A., Schwarz, J. P., Weigel, R., Fueglistaler, S., Prata, F. J., Vernier, J.-P., Schlager, H., Barnes, J. E., Antuña-Marrero, J.-C., Fairlie, D., Palm, M., Mahieu, E., Notholt, J., Rex, M., Bingen, C., Vanhellemont, F., Bourassa, A., Plane, J. M. C., Klocke, D., Carn, S. A., Clarisse, L., Trickl, T., Neely, R., James, A. D., Rieger, L., Wilson, J. C., and Meland, B.: Stratospheric aerosol – Observations, processes, and impact on climate, Rev. Geophys., 54, 278–335, doi: 10.1002/2015RG000511, 2016

Konopka, P., Grooß, J.-U., Plöger, F., and Müller, R.: Annual cycle of horizontal in-mixing into the lower tropical stratosphere, J. Geophys. Res. Atmos., 114, D19111, doi: 10.1029/2009JD011955, 2009.

Konopka, P., Grooß, J. U., Günther, G., Ploeger, F., Pommrich, R., Müller, R., and Livesey, N.: Annual cycle of ozone at and above the tropical tropopause: observations versus simulations with the Chemical Lagrangian Model of the Stratosphere (CLaMS), Atmos. Chem. Phys., 10, 121-132, doi: 10.5194/acp-10-121-2010, 2010.

Kravitz, B., and Robock, A., : Climate effects of high-latitude volcanic eruptions: Role of the time of year, J. Geophys. Res., 116, D01105, doi: 10.1029/2010JD014448, 2011.

Kravitz, B., Robock, A., Bourassa, A., Deshler, T., Wu, D., Mattis, I., Finger, F., Hoffmann, A., Ritter, C., Bitar, L., Duck, T. J., and Barnes, J. E.: Simulation and observations of stratospheric aerosols from the 2009 Sarychev volcanic eruption, J. Geophys. Res. Atmos., 116, D18211, doi: 10.1029/2010JD015501, 2011.

Klüser, L., Erbertseder, T., and Meyer-Arnek, J.: Observation of volcanic ash from Puyehue–Cordón Caulle with IASI, Atmos. Meas. Tech., 6, 35-46, doi:10.5194/amt-6-35-2013, 2013.

Levin, B. W., Rybin, A. V., Vasilenko, N. F., Prytkov, A. S., Chibisova, M. V., Kogan, M. G., Steblov, G. M., and Frolov, D. I.: Monitoring of the eruption of the Sarychev Peak Volcano in Matua Island in 2009 (central Kurile islands), Dokl. Earth Sci., 435, 1507-1510, doi: 10.1134/s1028334x10110218, 2010.

Manktelow, P. T., Carslaw, K. S., Mann, G. W., and Spracklen, D. V.: Variable CCN formation potential of regional sulfur emissions, Atmos. Chem. Phys., 9, 3253-3259, doi: 10.5194/acp-9-3253-2009, 2009.

Neely, R. R., Toon, O. B., Solomon, S., Vernier, J. P., Alvarez, C., English, J. M., Rosenlof, K. H., Mills, M. J., Bardeen, C. G., Daniel, J. S., and Thayer, J. P.: Recent anthropogenic increases in SO2 from Asia have minimal impact on stratospheric aerosol, Geophys. Res. Lett., 40, 999-1004, doi: 10.1002/grl.50263, 2013.

Niemeier, U., Timmreck, C., Graf, H. F., Kinne, S., Rast, S., and Self, S.: Initial fate of fine ash and sulfur from large volcanic eruptions, Atmos. Chem. Phys., 9, 9043-9057, doi: 10.5194/acp-9-9043-2009, 2009.

Oman, L., Robock, A., Stenchikov, G. L., and Thordarson, T.: High-latitude eruptions cast shadow over the African monsoon and the flow of the Nile, Geophys. Res. Lett., 33, L18711, doi: 10.1029/2006GL027665, 2006.

Pausata, F. S. R., Chafik, L., Caballero, R., and Battisti, D. S.: Impacts of high-latitude volcanic eruptions on ENSO and AMOC, Proc. Natl. Acad. Sci. U.S.A., 112, 13784-13788, doi: 10.1073/pnas.1509153112, 2015.

Ploeger, F., Gottschling, C., Griessbach, S., Grooß, J. U., Guenther, G., Konopka, P., Müller, R., Riese, M., Stroh, F., Tao, M., Ungermann, J., Vogel, B., and von Hobe, M.: A potential vorticity-based determination of the transport barrier in the Asian summer monsoon anticyclone, Atmos. Chem. Phys., 15, 13145-13159, doi: 10.5194/acp-15-13145-2015, 2015.

Ploeger, F., Günther, G., Konopka, P., Fueglistaler, S., Müller, R., Hoppe, C., Kunz, A., Spang, R., Grooß, J. U., and Riese, M.: Horizontal water vapor transport in the lower stratosphere from subtropics to high latitudes during boreal summer, J. Geophys. Res. Atmos., 118, 8111-8127, doi: 10.1002/jgrd.50636, 2013.

Randel, W. J., and Park, M.: Deep convective influence on the Asian summer monsoon anticyclone and associated tracer variability observed with Atmospheric Infrared Sounder (AIRS), J. Geophys. Res. Atmos., 111, D12314, doi: 10.1029/2005JD006490, 2006.

Ridley, D. A., Solomon, S., Barnes, J. E., Burlakov, V. D., Deshler, T., Dolgii, S. I., Herber, A. B., Nagai, T., Neely, R. R., Nevzorov, A. V., Ritter, C., Sakai, T., Santer, B. D., Sato, M., Schmidt, A., Uchino, O., and Vernier, J. P.: Total volcanic stratospheric aerosol optical depths and implications for global climate change, Geophys. Res. Lett., 41, 7763-7769, doi: 10.1002/2014GL061541, 2014.

Robock, A.: Volcanic eruptions and climate, Rev. Geophys., 38, 191-219, 10.1029/1998RG000054, 2000.

Robock, A.: The Latest on Volcanic Eruptions and Climate, Eos, Trans. Am. Geophys. Union, 94, 305-306, doi: 10.1002/2013EO350001, 2013.

Rodriguez, J. M., Ko, M. K. W., and Sze, N. D.: Role of the heterogeneous conversion of N2O5 on sulfate aerosols in global ozone losses, Nature, 352, 134-137, doi: 10.1038/352134a0, 1991.

Rybin, A., Chibisova, M., Webley, P., Steensen, T., Izbekov, P., Neal, C., and Realmuto, V.: Satellite and ground observations of the June 2009 eruption of Sarychev Peak volcano, Matua Island, Central Kuriles, Bull. Volcanol., 73, 1377-1392, doi: 10.1007/s00445-011-0481-0, 2011.

Santer, B. D., Bonfils, C., Painter, J. F., Zelinka, M. D., Mears, C., Solomon, S., Schmidt, G. A., Fyfe, J. C., Cole, J. N. S., Nazarenko, L., Taylor, K. E., and Wentz, F. J.: Volcanic contribution to decadal changes in tropospheric temperature, Nature Geosci., 7, 185-189, doi: 10.1038/ngeo2098, 2014.

Schmidt, A., Carslaw, K. S., Mann, G. W., Wilson, M., Breider, T. J., Pickering, S. J., and Thordarson, T.: The impact of the 1783–1784 AD Laki eruption on global aerosol formation processes and cloud condensation nuclei, Atmos. Chem. Phys., 10, 6025-6041, doi: 10.5194/acp-10-6025-2010, 2010.

Seviour, W. J. M., Butchart, N., Hardiman, S. C.: The Brewer–Dobson circulation inferred from ERA-Interim. Q. J. R. Meteorol. Soc., 138: 878–888. doi:10.1002/qj.966, 2012.

Solomon, S., Daniel, J. S., Neely, R. R., Vernier, J.-P., Dutton, E. G., and Thomason, L. W.: The Persistently Variable "Background" Stratospheric Aerosol Layer and Global Climate Change, Science, 333, 866-870, doi: 10.1126/science.1206027, 2011.

Solomon, S., Ivy, D. J., Kinnison, D., Mills, M. J., Neely R. R., Schmidt, A.: Emergence of healing in the Antarctic ozone layer. Science, doi: http://dx.doi.org/10.1126/science.aae0061, 2016.

Solomon, S., Sanders, R. W., Garcia, R. R., and Keys, J. G.: Increased chlorine dioxide over Antarctica caused by volcanic aerosols from Mount-Pinatubo, Nature, 363, 245-248, doi: 10.1038/363245a0, 1993.

Stohl, A., Forster, C., Frank, A., Seibert, P., and Wotawa, G.: Technical note: The Lagrangian particle dispersion model FLEXPART version 6.2, Atmos. Chem. Phys., 5, 2461-2474, doi:10.5194/acp-5-2461-2005, 2005.

Tilmes, S., Muller, R., and Salawitch, R.: The sensitivity of polar ozone depletion to proposed geoengineering schemes, Science, 320, 1201-1204, doi: 10.1126/science.1153966, 2008.

Timmreck, C.: Modeling the climatic effects of large explosive volcanic eruptions, WIREs Clim. Change, 3, 545-564, doi: 10.1002/wcc.192, 2012.

Vernier, J. P., Thomason, L. W., Pommereau, J. P., Bourassa, A., Pelon, J., Garnier, A., Hauchecorne, A., Blanot, L., Trepte, C., Degenstein, D., and Vargas, F.: Major influence of tropical volcanic eruptions on the stratospheric aerosol layer during the last decade, Geophys. Res. Lett., 38, L12807, doi: 10.1029/2011GL047563, 2011.

von Glasow, R., Bobrowski, N., and Kern, C.: The effects of volcanic eruptions on atmospheric chemistry, Chem. Geol., 263, 131–142, doi: http://dx.doi.org/10.1016/j.chemgeo.2008.08.020, 2009.

von Savigny, C., Ernst, F., Rozanov, A., Hommel, R., Eichmann, K. U., Rozanov, V., Burrows, J. P., and Thomason, L. W.: Improved stratospheric aerosol extinction profiles from SCIAMACHY: validation and sample results, Atmos. Meas. Tech., 8, 5223-5235, doi: 10.5194/amt-8-5223-2015, 2015.

Atmos. Chem. Phys. Discuss., doi:10.5194/acp-2017-425, 2017
Manuscript under review for journal Atmos. Chem. Phys.
Discussion started: 19 May 2017

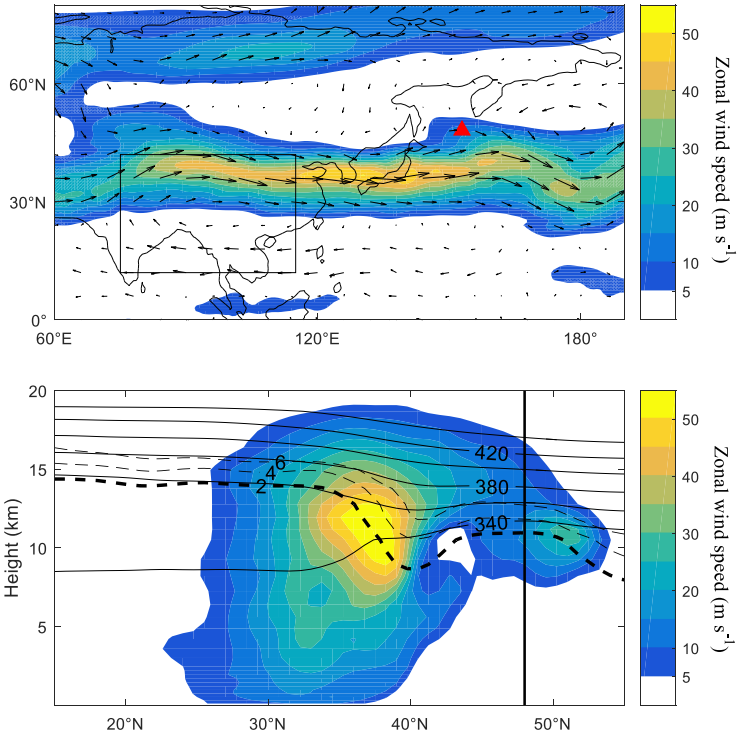

Figure 1: Top: zonal wind (shaded) and wind vectors on the 370 K isentropic surface at 0 UTC on 12 June 2009. The location of the Sarychev peak is denoted with a red triangle. The black rectangle indicats the area of developing ASM anticyclone. Bottom: vertical section of zonal wind (shaded) and contours of potential temperature from 340 K to 440 K (black solid lines) and potential vorticity from 2 PVU to 6 PVU (black dashed lines) along 153°E. The vertical black line denotes the latitude (48.1°N) of the Sarychev peak.

Atmos. Chem. Phys. Discuss., doi:10.5194/acp-2017-425, 2017
Manuscript under review for journal Atmos. Chem. Phys.
Discussion started: 19 May 2017

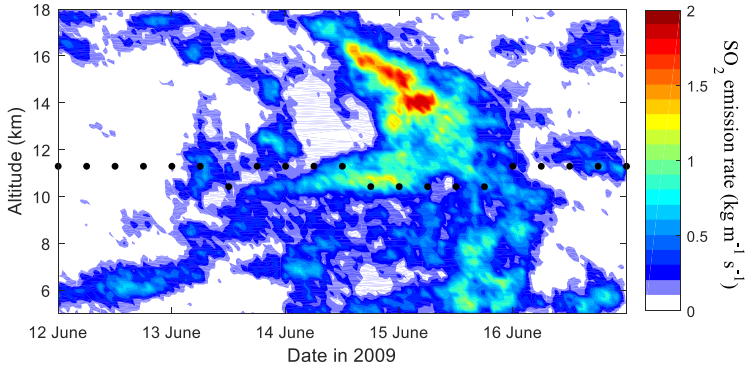

Figure 2: Sarychev SO_2 emission time series derived with AIRS measurements using a backward trajectory approach. The emission data is binned every 1 hour and 0.2 km. Black dots denote the height of the thermal tropopause.

Atmos. Chem. Phys. Discuss., doi:10.5194/acp-2017-425, 2017
Manuscript under review for journal Atmos. Chem. Phys.
Discussion started: 19 May 2017

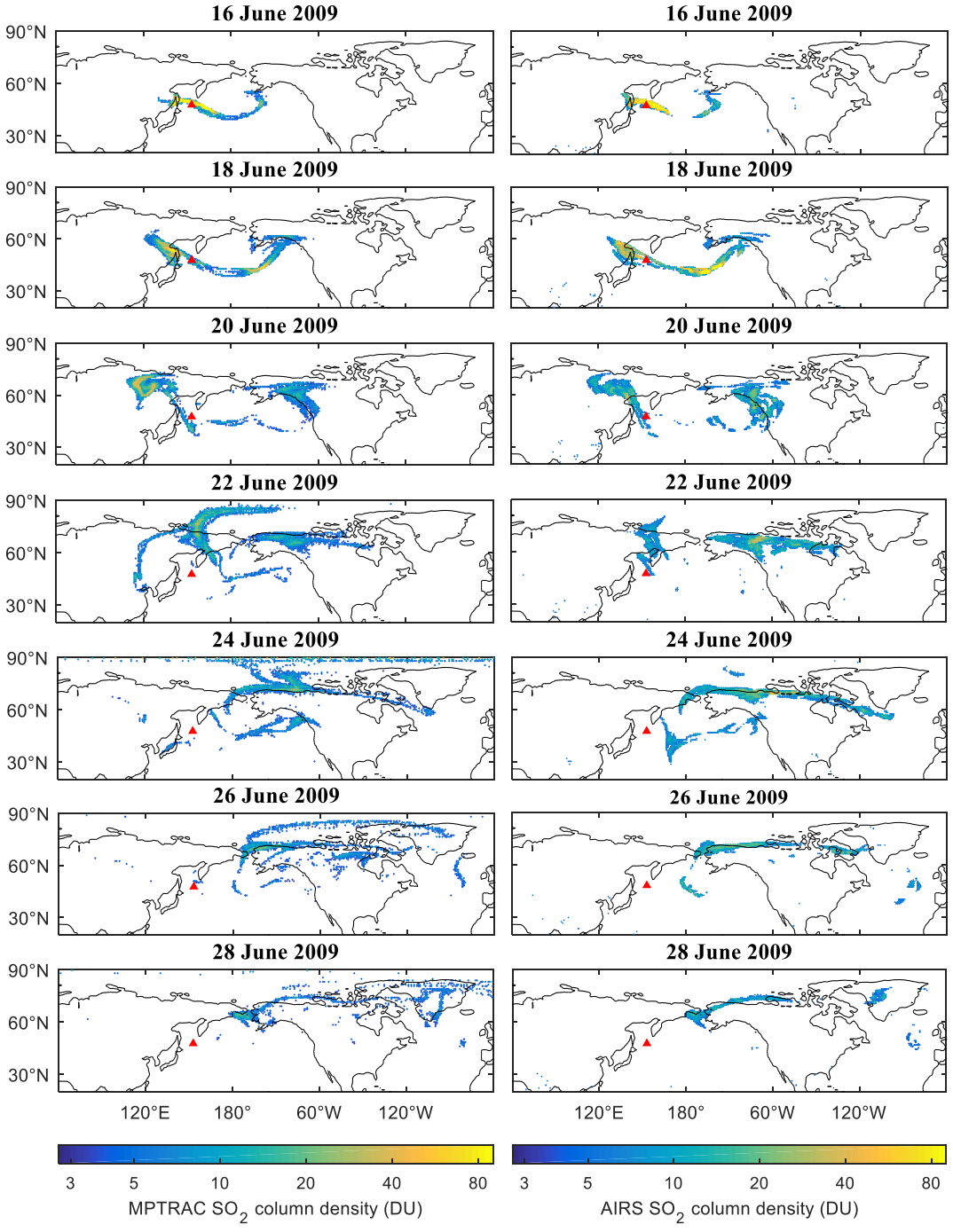

Figure 3: The evolution of SO_2 column density from MPTRAC (left, in Dobson units) and SO_2 column density from AIRS (right) for the period 16–28 June 2009. The MPTRAC SO_2 column density are shown for 0 UTC on selected days and AIRS data are collected within ± 6 hours. Only values larger than 2 DU are shown. The red triangle denotes the location of the Sarychev peak.

Atmos. Chem. Phys. Discuss., doi:10.5194/acp-2017-425, 2017
Manuscript under review for journal Atmos. Chem. Phys.
Discussion started: 19 May 2017

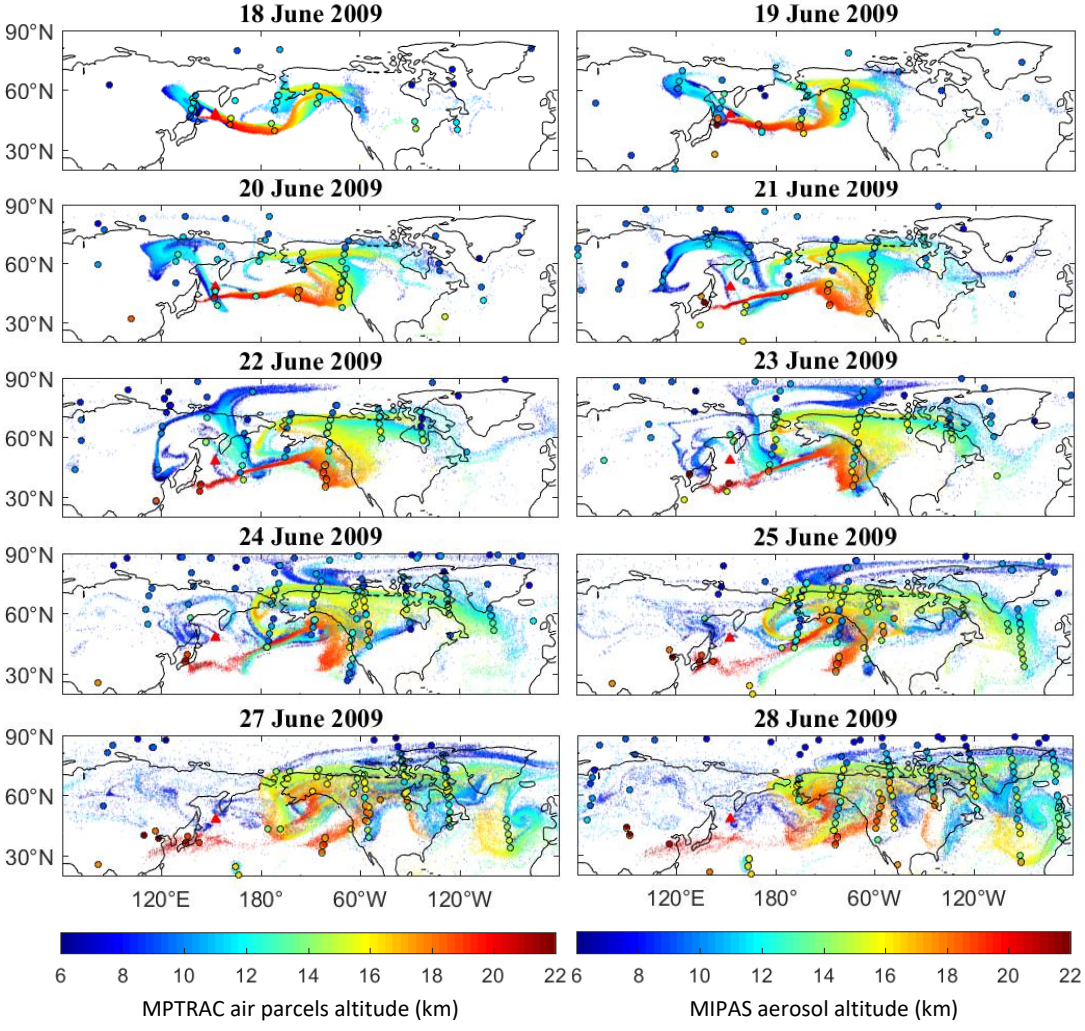

Figure 4: The evolution of SO_2 air parcel altitudes from MPTRAC (shown for 0 UTC on selected days) and MIPAS aerosol detections within ± 6 hours, denoted with color-filled circle markers. The altitudes of all air parcels, regardless of their SO_2 values, are shown. The red triangle denotes the location of the Sarychev peak.

Atmos. Chem. Phys. Discuss., doi:10.5194/acp-2017-425, 2017
Manuscript under review for journal Atmos. Chem. Phys.
Discussion started: 19 May 2017

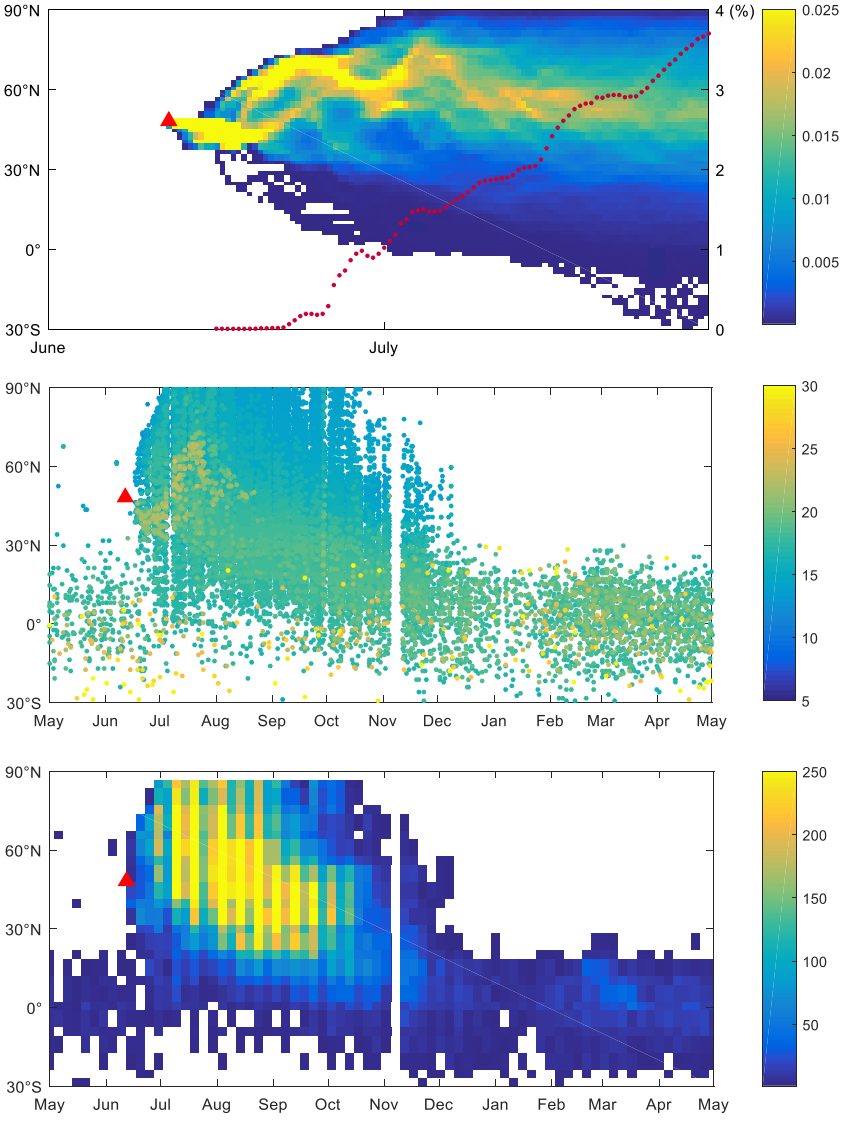

Figure 5: Top: Percentage (%) of air parcels above 380 K from MPTRAC simulation binned every 12 hours and 2° in latitude. Red dots denote the percentage of air parcels between 30°N and 30°S. Middle: MIPAS aerosol altitudes (km) above 380K from May 2009 to April 2010. Bottom: number of MIPAS aerosol detections. Detections are binned every 5 days and 5° in latitude. The red triangle denotes the time and latitude of the first Sarychev eruption.

Atmos. Chem. Phys. Discuss., doi:10.5194/acp-2017-425, 2017
Manuscript under review for journal Atmos. Chem. Phys.
Discussion started: 19 May 2017

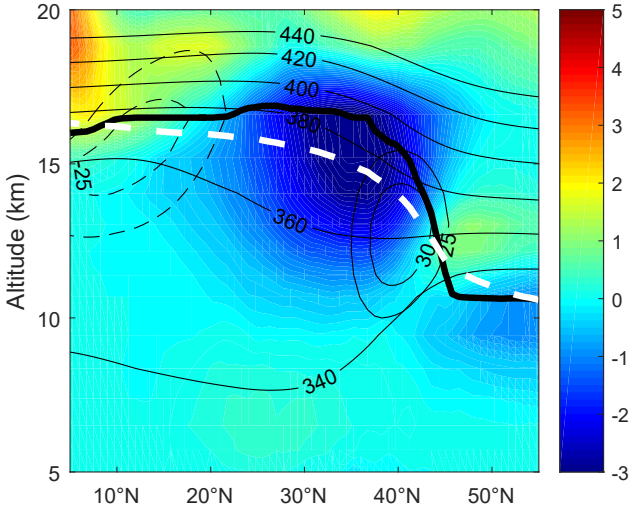

Figure 6: Zonal mean PV anomaly (shaded) in the Asian monsoon anticyclone (40–120°E) with respect to the zonal mean, averaged over 2009 summer (June-August). Zonal wind (black, solid/dashed positive/negative) is averaged between 40 and 120°E. The first thermal tropopause zonally averaged over 0 - 360°E is shown as dashed white line, averaged over 40 to 120°E as thick black line.

Atmos. Chem. Phys. Discuss., doi:10.5194/acp-2017-425, 2017
Manuscript under review for journal Atmos. Chem. Phys.
Discussion started: 19 May 2017

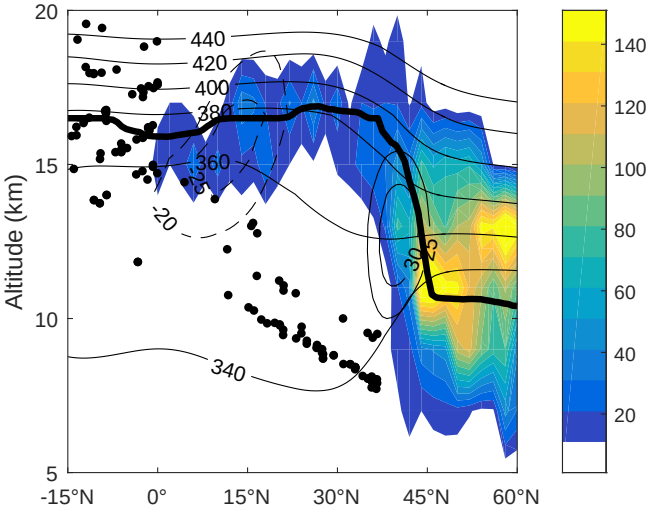

Figure 7: Number of MIPAS aerosol detections between 40°E and 120°E during June-August 2009 (binned every 2 km in altitude and 2° in latitude). Sparse detections (number of detections in each bin is smaller than 10) are shown with black dots. The tropopause, potential temperature, and zonal wind are same as shown in Fig. 6.

Atmos. Chem. Phys. Discuss., doi:10.5194/acp-2017-425, 2017
Manuscript under review for journal Atmos. Chem. Phys.
Discussion started: 19 May 2017

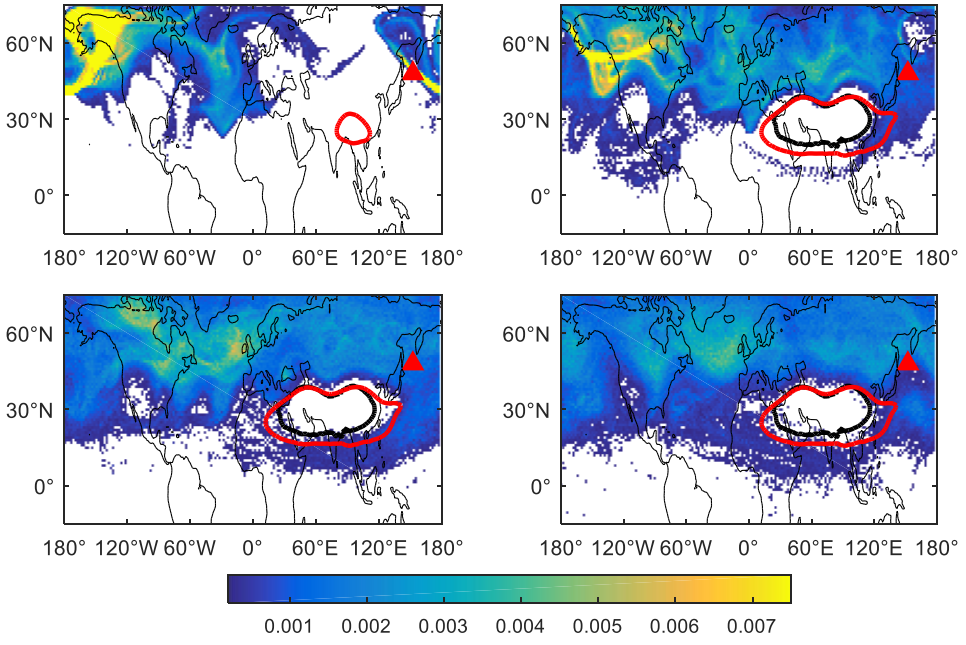

Figure 8: Percentage (%) of air parcels by 30 June (top left), 10 July (top right), 20 July (bottom left) and 31 July 2009 (bottom right) between 360 and 400 K from MPTRAC simulations. Results are binned every 2° in longitude and 1° in latitude. The 14,320 geopotential height (m) on 150 hPa is marked in red and the PV-based barrier on 370 K is marked in black. The red triangle denotes the location of the Sarychev.

Atmos. Chem. Phys. Discuss., doi:10.5194/acp-2017-425, 2017
Manuscript under review for journal Atmos. Chem. Phys.
Discussion started: 19 May 2017

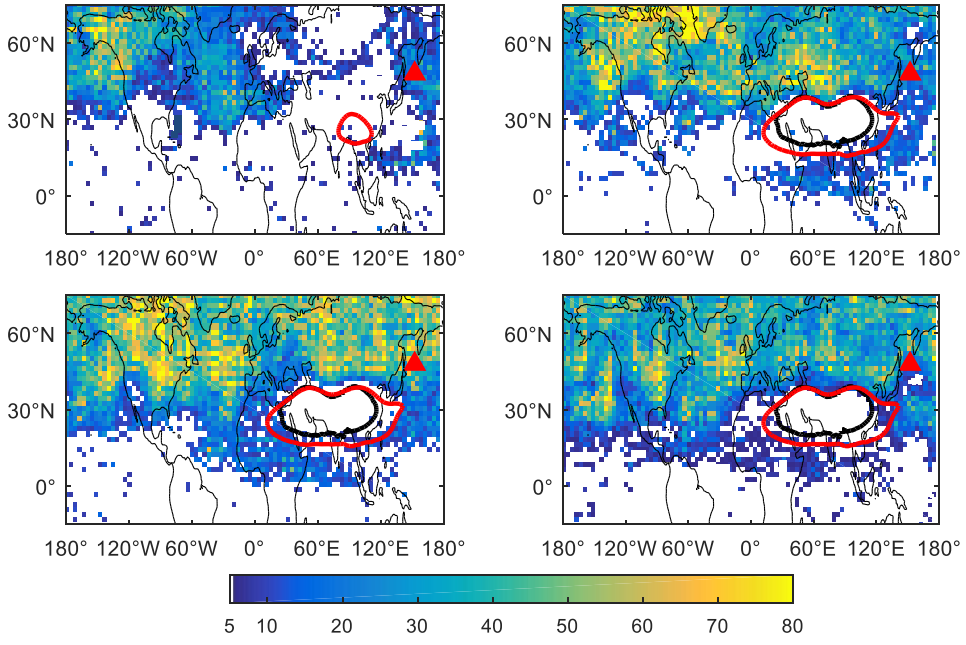

Figure 9: Number of MIPAS aerosol detections and aerosol data generated with 1.5-day forward and 1.5-day backward trajectory calculation, by 30 June (top lest), 10 July (top right), 20 July (bottom left) and 31 July (bottom right) between 360 and 400 K. Results are binned every 4° in longitude and 2° in latitude. The 14,320 geopotential height (m) on 150 hPa is marked in red and the PV-based barrier on 370 K is marked in black. Red triangle denotes the location of Sarychev.

Atmos. Chem. Phys. Discuss., doi:10.5194/acp-2017-425, 2017
Manuscript under review for journal Atmos. Chem. Phys.
Discussion started: 19 May 2017

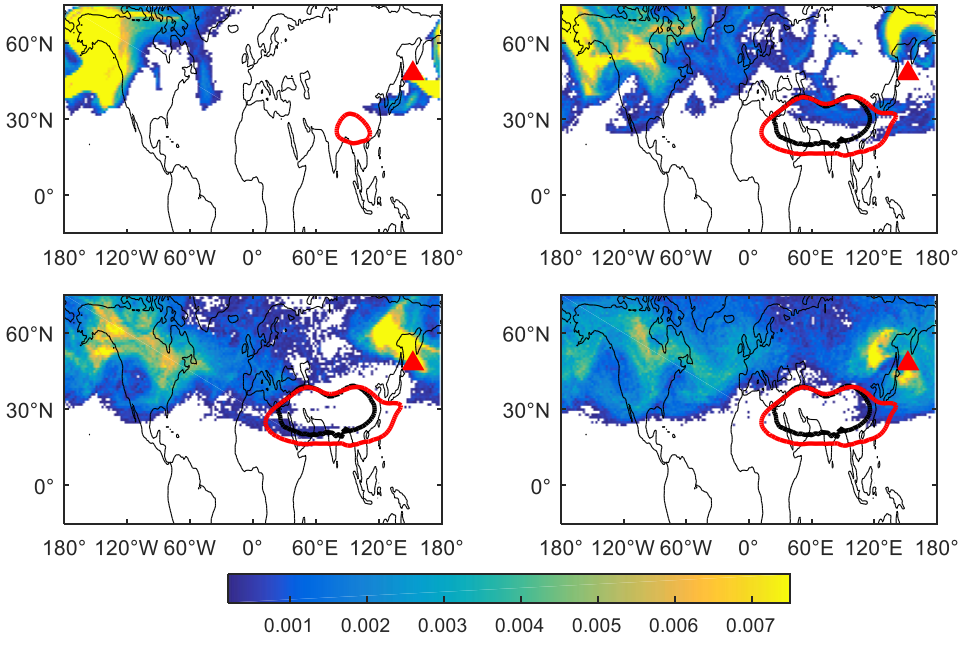

Figure 10: Same as Fig. 8 but for percentage (%) of total air parcels above 400 K.

Atmos. Chem. Phys. Discuss., doi:10.5194/acp-2017-425, 2017
Manuscript under review for journal Atmos. Chem. Phys.
Discussion started: 19 May 2017

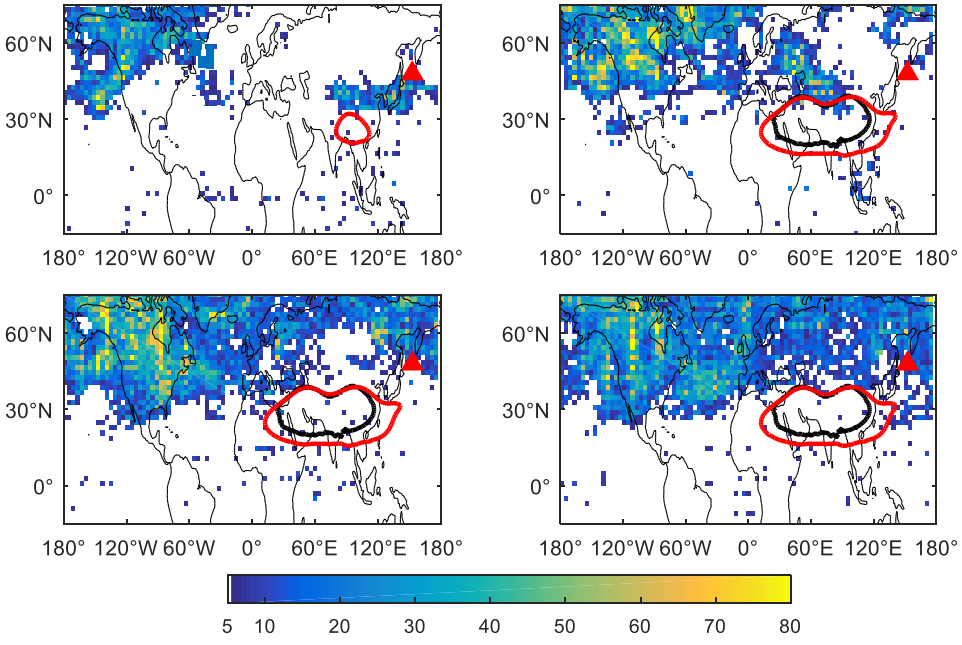

Figure 11: Same as Fig. 9, but for number of detections above 400 K.

Atmos. Chem. Phys. Discuss., doi:10.5194/acp-2017-425, 2017
Manuscript under review for journal Atmos. Chem. Phys.
Discussion started: 19 May 2017

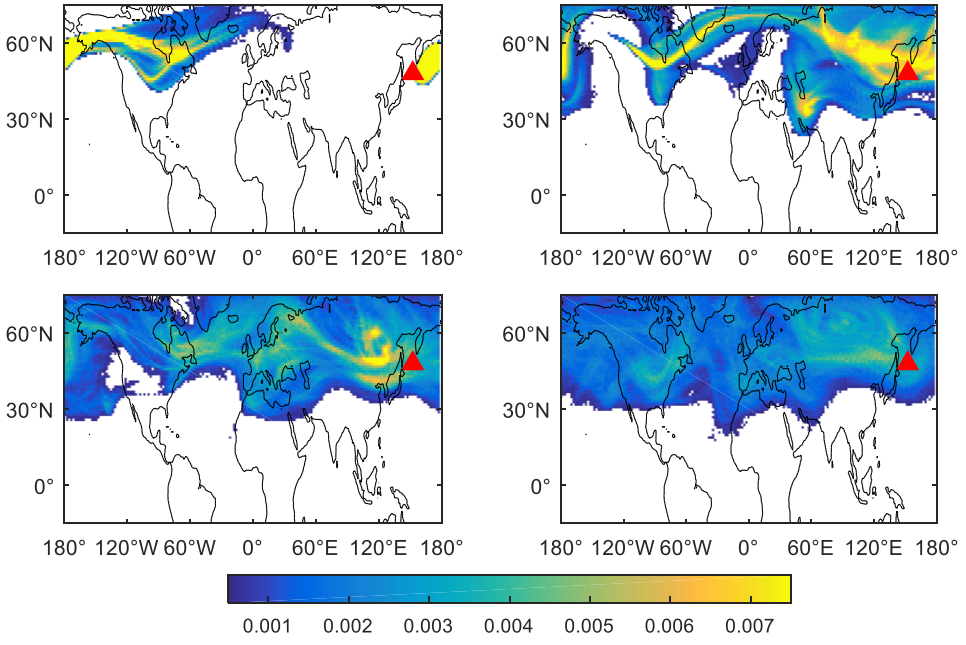

Figure 12: Percentage (%) of air parcels for the wintertime sensitivity study, by 10 January (top left), 20 January (top right), 31 January (bottom left) and 10 February 2009 (bottom right) from an MPTRAC simulation for a hypothetical eruption of the Sarychev between 360 and 400 K. Results are binned every 2° in longitude and 1° in latitude. Red triangle denotes the location of Sarychev.

Atmos. Chem. Phys. Discuss., doi:10.5194/acp-2017-425, 2017
Manuscript under review for journal Atmos. Chem. Phys.
Discussion started: 19 May 2017

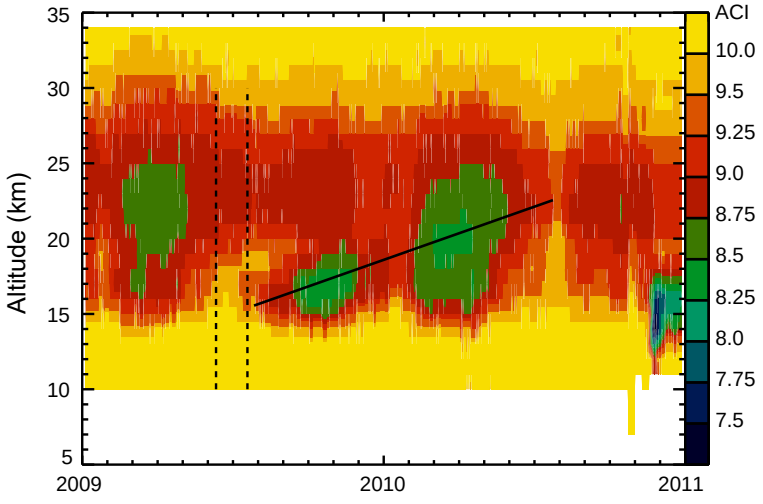

Figure 13: 9-day running median of aerosol-cloud-index (ACI) between 10°N and 10°S from 2009 to 2010. Ascent speed of the water vapour tape recorder (solid line) is derived from Glanville et al., 2016 using MLS observations. Black dashed lines indicate the eruption date and 20 July when the simulations show first substantial transport to 10°N–10°S.